

Joint Communication and Sensing: 5G NR Compliant Ranging Using the Sounding Reference Signal

Michael Hofstadler, *Student Member, IEEE*, Reinhard Feger, Andreas Springer, *Member, IEEE*, Andreas Stelzer, *Member, IEEE*, Harald Pretl, *Senior Member, IEEE*

Abstract—In this work, a proof of concept for 5G-compliant user-equipment side sensing is presented. It is based on orthogonal frequency division multiplexing radar-based ranging which is realized in this work by using the sounding reference signal from the 5G New Radio standard. The signal configuration and thus the corresponding waveform is generated in compliance with the existing 3rd Generation Partnership Project standard for 5G. It is an uplink physical signal and is originally intended, amongst others, for channel estimation. The used model is introduced, followed by the sounding reference signal. This leads to a first proof of concept by presenting simulation and measurement results. We show, that a range estimation error in the order of centimeters is achievable.

Index Terms—5G, integrated sensing and communications, joint communication and sensing, joint radar-communications, mmWave, New Radio, OFDM, radar, range estimation, sounding reference signal.

I. INTRODUCTION

WITH the consecutive release of standards for broadband cellular networks, like 5G and its predecessor, both new challenges and opportunities arise. One prominent example for this is the introduction of the so-called frequency range 2 (FR2) in 5G ranging from 24.25 to 52.6 GHz [1]. The increased bandwidths available in FR2 provide a promising base for new opportunities in terms of sensing, with an even increasing trend towards 6G. This is also reflected by the popularity gaining research area of joint communication and sensing (JCAS) [2], also known as joint radar-communications (JRC), which can be seen, e.g., in the appearance of the first two editions of the IEEE JC&S Symposium [3]. Although research for bringing communication and sensing together exist for a while already [4], a large number of new research efforts within the different areas of JCAS can be found nowadays. The majority of them address an area of vehicular side [5], or network side JCAS, addressing a variety of scopes, from more general, network-wide concepts [6], to the analysis of JCAS performance within a base station (BS) [7]. Less

Manuscript received Month Day, Year; revised Month Day, Year.

Michael Hofstadler, Reinhard Feger, Andreas Springer and Andreas Stelzer are with the Institute for Communications Engineering and RF-Systems, Johannes Kepler University, Linz 4040, Austria (e-mail: michael.hofstadler@jku.at; reinhard.feger@jku.at; andreas.springer@jku.at; andreas.stelzer@jku.at). Harald Pretl is with the Institute for Integrated Circuits, Johannes Kepler University, Linz 4040, Austria (e-mail: harald.pretl@jku.at)

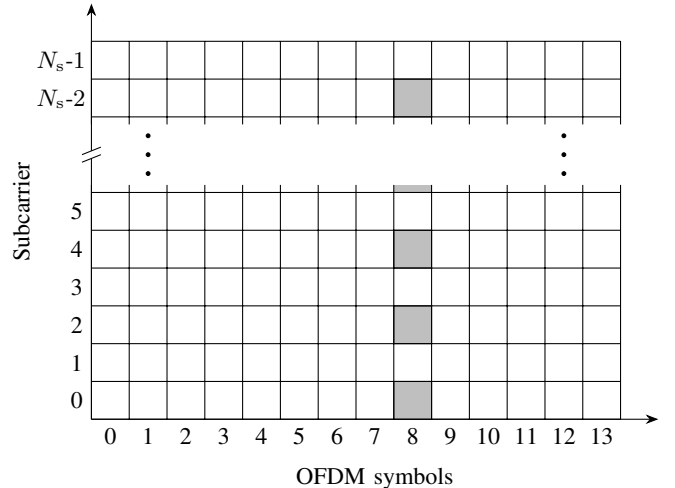


Fig. 1. A slot of the radio frame from the resource grid. In the OFDM symbol number eight, every second subcarrier is occupied by a complex-valued symbol, denoted by the gray filled squares.

research effort, on the other hand, goes to user equipment (UE) side JCAS. Reference [8] investigates UE side JCAS for grid-based indoor mapping, utilizing a New Radio (NR) uplink transmit signal.

In this work, we present a UE side JCAS approach. We focus on embedding ranging into an existing 5G communication scenario. Thus we need to be fully compliant with the 5G NR standard as released by the 3rd Generation Partnership Project (3GPP) [1], [9]. Therefore, it is obvious that we perform ranging based on an orthogonal frequency division multiplexing (OFDM) radar, which is already well established [10]. Having the UE side in scope, the used signal has to be an uplink (UL) signal. Here we propose to use the sounding reference signal (SRS). This signal was chosen for a number of reasons, which will be illustrated in the following section.

II. OFDM-BASED RANGING AND THE SOUNDING REFERENCE SIGNAL

The UE is regularly communicating with a BS when connected to the network. Even if no user data is actively transferred, the link partners, i.e. BS and UE, regularly send pilot signals, like control-, synchronization-, and sounding-signals. Ranging at the UE can be performed if the reflections

of UL pilot signals stemming from objects in the vicinity are received and processed properly.

Before we elaborate on the chosen UL pilot signal we will introduce the 5G NR frame- and resource structure and the principle of OFDM-based ranging.

A. 5G NR Frame- and Resource Structure

The available time and frequency resources in an OFDM-based mobile communication network are organized in a resource grid. This grid is a matrix of resource grid elements, where the rows k represent the individual subcarriers, i.e. the frequency resources, whereas columns l represent the OFDM symbols according to the time resources. In the time domain, OFDM symbols are grouped into slots and slots are grouped into subframes which are grouped into a radio frame. In this work only a single slot is taken into account, as this is the smallest interval for consecutive OFDM symbols.¹ The subcarrier spacing Δf and thus the OFDM symbol duration, the cyclic prefix length and the number of OFDM symbols per slot are defined by the so-called numerology μ [1]. The subcarrier spacing Δf is given by

$$\Delta f = 2^\mu \cdot 15 \text{ kHz}. \quad (1)$$

For this work $\mu = 3$ is selected, which results in a subcarrier spacing of $\Delta f = 120$ kHz. For the chosen μ a slot comprises 14 OFDM symbols.

If a resource grid element is occupied, it is associated with a complex-valued OFDM transmission symbol $a_{k,l}$ with $|a_{k,l}| > 0$. In all unoccupied resource grid elements $a_{k,l} = 0$. Fig. 1 shows the resource grid of one slot, where every second subcarrier of the OFDM symbol number eight is occupied. All other resource grid elements are unoccupied.

B. OFDM-Based Ranging

The complex-valued symbols for the resource grid elements are given by $a_{k,l} = A_{k,l} e^{j\Psi_{k,l}}$, where $A_{k,l} \in \mathbb{R}$ is the amplitude and $\Psi_{k,l}$ is the phase of the complex-valued symbol. The continuous-time OFDM baseband signal $s_l(t)$ transmitted by the UE, including the cyclic prefix, for the l th OFDM symbol and N_s subcarriers is given by [9]

$$s_l(t) = \begin{cases} \bar{s}_l(t) & 0 \leq t < T_s \\ 0 & \text{otherwise} \end{cases} \quad (2)$$

with

$$\bar{s}_l(t) = \sum_{k=0}^{N_s-1} a_{k,l} e^{j2\pi(k-N_s/2)\Delta f(t-T_{cp})}, \quad (3)$$

where $T_s = T_{\text{symb}} + T_{cp}$ is the sum of the symbol time duration $T_{\text{symb}} = 1/\Delta f$ and the cyclic prefix time duration T_{cp} . For the sake of simplicity, compared to [9], the subcarrier starting point k_0 and the starting point in time t_{start} has been set to zero and the antenna port p has been set to one. From (2) we can compute the radio frequency (RF) signal

$s(t)$ transmitted at the carrier frequency f_0 with the amplitude scaling factor β as

$$s(t) = \text{Re}\{\beta s_l(t) e^{j2\pi f_0(t-T_{cp})}\}. \quad (4)$$

We assume the transmitted signal in (4) to be reflected by an object. Thus the signal $x(t)$ received by the UE is a scaled (by α) and delayed (by τ , which depends on the distance between UE and object) version of the TX signal corrupted by noise $n(t)$.

$$x(t) = \alpha s(t - \tau) + n(t) \quad (5)$$

After downconversion, cyclic prefix removal and demodulation, the k th subcarrier element of the l th OFDM symbol of the baseband signal is given by

$$X_l[k] = \alpha \beta A_{k,l} e^{j(\Psi_{k,l} - 2\pi\tau\{k\Delta f + f_0\})} + N'_k, \quad (6)$$

where N'_k represents the processed noise.

The range R between the UE and the object is related to τ and the speed of light in the corresponding medium c by $R = c\tau/2$. To estimate τ and thus R , the baseband signal X_l needs to be further processed to extract the range information.

To remove the individual phase and amplitude information coming from the complex-valued transmission OFDM symbols $a_{k,l}$, an element-wise division is applied to arrive at

$$\varepsilon_l[k] = \frac{X_l[k]}{a_{k,l}} = \alpha \beta \gamma e^{-j2\pi\tau k\Delta f} + N_k. \quad (7)$$

where $\gamma = e^{-j2\pi\tau f_0}$, describes a phase offset constant over k .

To calculate the complex-valued range profile $\tilde{\rho}[n]$, a fast Fourier transform (FFT) along the subcarrier index k is performed with

$$\tilde{\rho}[n] = \sum_{k=0}^{N_{\text{FFT}}-1} \varepsilon_l[k] e^{j2\pi k\Delta f\tau_n}. \quad (8)$$

where N_{FFT} is the number of FFT points and $\tau_n = n/(N_{\text{FFT}}\Delta f)$ are the discretized time delay steps. According to the 3GPP standard an $N_{\text{FFT}} = 4096$ point FFT has been used. The range profile is then given by $\rho[n] = |\tilde{\rho}[n]|^2$. The estimated time delay $\tau_{\hat{n}}$, according to the peak position $\hat{n} = \arg \max_n \rho[n]$, then represents the nearest neighbor to the true time delay of $x(t)$ and the corresponding range R .

To increase the precision of the estimation, an interpolation based on the computationally efficient chirp-Z transform (CZT) can be performed [12]. The domain used for this operation is limited to the vicinity around the peak from $\tau_{\hat{n}-1}$ to $\tau_{\hat{n}+1}$. This interpolated range profile is denoted as $\rho_{\text{CZT}}[m]$. With N_{FFT} interpolation points, this leads to a more precise discretization of $\tau_m = 2m/(N_{\text{FFT}}^2\Delta f)$. The now received peak position $\hat{m} = \arg \max_m \rho_{\text{CZT}}[m]$ and the according time delay $\tau_{\hat{m}}$ is finally used to estimate the range \hat{R} to the object, which can be computed as

$$\hat{R} = \frac{c_0}{2} \tau_{\hat{m}}. \quad (9)$$

¹Here, we do not consider mini-slot transmission, which can be used for ultra-reliable low-latency communication [11].

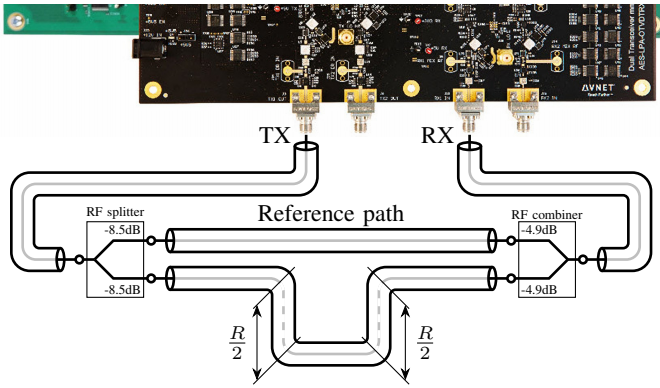


Fig. 2. The measurement setup with a cable-based measurement scenario. The RF network, based on coaxial components consist of two paths, connected by RF splitters/combiners. The reference path represents the TX/RX leakage and a longer, second path represents the distance to a target of interest. The dashed lines represents the difference in length R of the two paths.

C. The Sounding Reference Signal

The SRS is used, amongst others, for channel estimation in the UL. Therefore, it is also sent in situations when no user data is sent. It is based on a low peak-to-average power ratio (PAPR) sequence. Depending on the length of the sequence it is a Zadoff-Chu sequence, or a numerically derived sequence with properties which fulfill the requirements of the standard similarly as the Zadoff-Chu sequence does [9]. Therefore, the SRS sequence is a constant-amplitude zero-autocorrelation (CAZAC) sequence. The PAPR characteristic is also beneficial for the transmit signal, as the PAPR of the waveform is limited, and the requirements on the transceiver are lower, compared to an OFDM transmit signal carrying a random bit stream.

The sequence is allocated in the resource grid according to the comb number $K_{TC} \in \{2, 4, 8\}$. This number defines how every K_{TC} th subcarrier is used for SRS sequence allocation. A resource grid occupied by an SRS sequence with $K_{TC} = 2$ can be seen in Fig. 1. This also means, that even if the subcarrier spacing is $\Delta f = 120$ kHz, the smallest frequency difference for a single SRS sequence is $\min(K_{TC})\Delta f = 240$ kHz. The sequence can occupy $N_{\text{syimb}}^{\text{SRS}} \in \{1, 2, 4, 8, 10, 12, 14\}$ consecutive OFDM symbols per slot.

In terms of subcarriers, the number of resource elements which can be occupied ranges from 24 up to 1584 in a single-carrier configuration. The number of occupied subcarriers therefore also corresponds to the bandwidth of the signal.

The SRS is also used in the so-called *beam mobility procedure*. As beamforming is part of 5G NR, selecting the best beam for transmission is of high interest for both link partners. Within this UL procedure, the BS performs power measurements, while the UE is transmitting the SRS on one or more beams [13]. Thus, the SRS could be used in a similar manner for UE-side ranging.

III. EXPERIMENTAL VERIFICATION METHODS

To verify the concept of ranging with a 5G NR compliant signal, a software framework has been created. This framework has been used to create standard compliant carrier and SRS

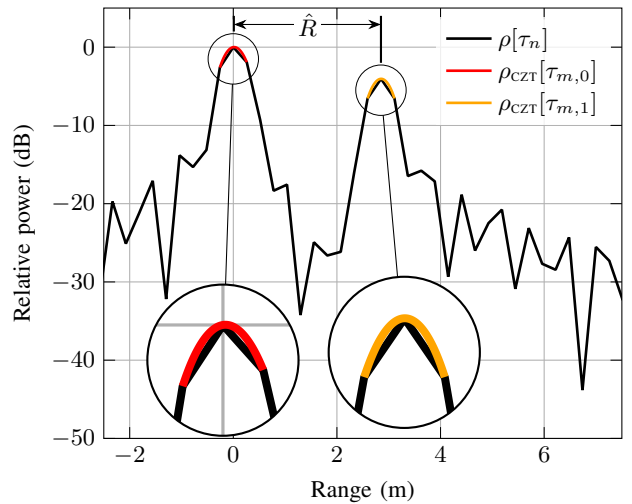


Fig. 3. The range profile $\rho[\tau_n]$, from the measurement results according to the setup with a path difference of $R = 2.76$ m, normalized to the strongest peak. The CZT interpolation around the peak for the reference path $\rho_{\text{CZT}}[\tau_{m,0}]$ is shown in red, the one around the peak caused by the second longer path $\rho_{\text{CZT}}[\tau_{m,1}]$ in orange. The distance between the two peaks is the estimated range \hat{R} .

configurations, and to generate standard compliant waveforms [14]. The framework has also been used for simulations. The simulated scenarios have been set to match the measurement setup, to allow comparison of the results. For the measurement setup, an *AMD-Xilinx RFSoc Gen 3 Kit for mmWave* with a configured carrier frequency of $f_0 = 25$ GHz has been used. The hardware has been controlled by the *Avnet RFSoc Explorer* software.

As there is no synchronization between TX and RX in the default Field Programmable Gate Array (FPGA) configuration, a reference target is introduced. The delay of the reference target was chosen to be shorter than the target of interest. This reference target is also motivated due to the fact, that in the UE, TX and RX are also not precisely synchronized, but a TX-to-RX leakage signals is present, which can be exploited for synchronization purposes. The two different targets and therefore the according time delays are denoted as $\tau_{m,i}$, where $i = \{0, 1\}$ is the index of the two most predominant peaks in the range profile. The estimated time delays are the one from the reference path $\tau_{\hat{m},0}$ and the one representing the target distance of interest $\tau_{\hat{m},1}$. The difference $\tau_{\hat{m},\delta} = \tau_{\hat{m},0} - \tau_{\hat{m},1}$ is then related to the distance between the reference target and the target of interest

$$\hat{R} = \frac{c_0}{2} \tau_{\hat{m},\delta}. \quad (10)$$

Fig. 2 shows the measurement setup. The measurements have been performed with a cable-based measurement scenario. The RF network, based on coaxial components, consists of two paths, connected by RF splitters/combiners. The reference path represents the TX/RX leakage and the longer, second path represent the distance to a target of interest. The dashed lines represents the difference in length R of the two paths. Therefore the relation between estimated range and time delay

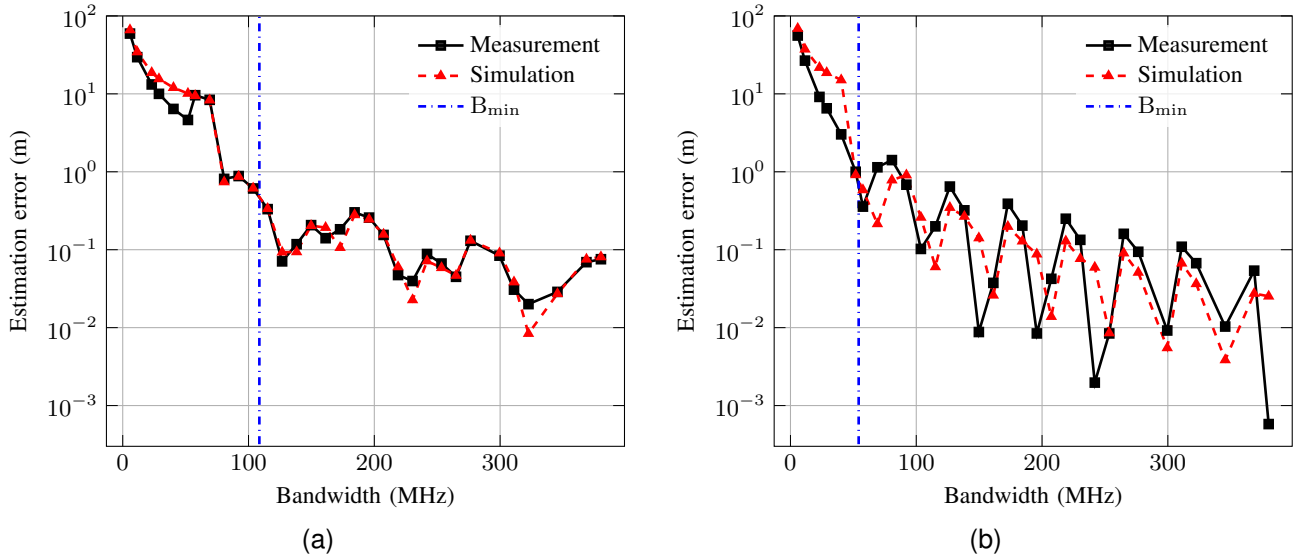


Fig. 4. The estimation error compared to the ground truth, for different signal bandwidths. The black solid line shows the results from the measurement and the red dashed line shows the results from the simulation. The blue dash dotted line represents the minimum bandwidth B_{\min} required to resolve the responses of reference and measurement path. The shown results correspond to RF networks with path differences of (a) $R = 2.76$ m and (b) $R = 5.53$ m.

changes to

$$\hat{R} = v_p \tau_{\hat{m}, \delta}, \quad (11)$$

where v_p is the phase velocity in the coaxial lines.

Because of the missing synchronization between TX and RX, a moving average filter, with a window size of T_s is applied on the RX signal to find the start position of the signal within the acquired data.

To determine the ground truth of the range of interest, the S-parameters for all used RF paths have been measured with a network analyzer.

IV. RESULTS

Fig. 3 shows the range profile $\rho[\tau_n]$, normalized to the strongest peak for a path difference of $R = 2.76$ m. Around the two detected peaks, the CZT results $\rho_{\text{CZT}}[\tau_{m,i}]$ are shown in red and orange. The distance between the two peaks is the estimated range \hat{R} . Fig. 4 shows the estimation error $|R - \hat{R}|$ from both the measurement setup and the according simulation as function of the bandwidth of the SRS. We also show the minimum bandwidth B_{\min} which allows to resolve the peaks stemming from the reference and the measurement path $B_{\min} \geq c_0/R$. Fig. 4(a) shows the results from the measurement configuration with a path length difference of $R = 2.76$ m and Fig. 4(b) for a configuration with $R = 5.53$ m. For SRS signals with a bandwidth smaller than B_{\min} , the used peak detection algorithm could not distinguish the peaks in most of the cases. Therefore the next biggest side lobe was wrongly identified as target, resulting in an estimation error in the range of several tens of meters. Starting from a SRS configuration with B_{\min} the estimation error is in the order of meters and reduces to the order of centimeters in Fig. 4(a) and even to the order of millimeters in Fig. 4(b) for bandwidths beyond 200 MHz. The almost periodic variation in the estimation error results from the fact, that for each of the

two paths in the setup, according to (7) a sinusoidal oscillation is present over a limited amount of subcarriers. Each results in a sinc in the range profile. Thus, the sidelobes of one sinc interfere with the main lobe of the other.

V. CONCLUSION

This paper discussed a OFDM-based ranging concept, which adheres to the 5G NR 3GPP standard. At first the basic OFDM model was introduced, whereas later-on the standard-related details have been highlighted. The SRS was introduced as 5G compliant signal and according waveform of choice. The measurement setup and the simulations have been explained and finally the results have been presented in Sec. IV. Range profiles have been presented together with results of the estimation error for two different measurement setups. We demonstrated, that a ranging estimation error in the order of centimeters is achievable if the SRS is configured with sufficient bandwidth.

ACKNOWLEDGMENTS

The financial support by the Austrian Federal Ministry for Digital and Economic Affairs, the National Foundation for Research, Technology and Development and the Christian Doppler Research Association is gratefully acknowledged.

REFERENCES

- [1] 3GPP, "User Equipment (UE) radio transmission and reception; Part 2: Range 2 Standalone," 3rd Generation Partnership Project (3GPP), Technical Specification (TS) 38.101-2, 1 2022, version 17.5.0. [Online]. Available: <https://portal.3gpp.org/desktopmodules/Specifications/SpecificationDetails.aspx?specificationId=3284>
- [2] M. Nemati, Y. H. Kim, and J. Choi, "Toward Joint Radar, Communication, Computation, Localization, and Sensing in IoT," *IEEE Access*, vol. 10, pp. 11 772–11 788, 2022.
- [3] *2nd IEEE International Hybrid Symposium on Joint Communications & Sensing*. [Online]. Available: <https://jcms-symposium.org>

- [4] P. Hughes and J. Choe, "Overview of advanced multifunction RF system (AMRFS)," in *Proceedings 2000 IEEE International Conference on Phased Array Systems and Technology (Cat. No.00TH8510)*, 2000, pp. 21–24.
- [5] H. Wymeersch, G. Seco-Granados, G. Destino, D. Dardari, and F. Tufvesson, "5G mmWave Positioning for Vehicular Networks," *IEEE Wireless Communications*, vol. 24, no. 6, pp. 80–86, 2017.
- [6] T. Wild, V. Braun, and H. Viswanathan, "Joint Design of Communication and Sensing for Beyond 5G and 6G Systems," *IEEE Access*, vol. 9, pp. 30 845–30 857, 2021.
- [7] F. Dong, W. Wang, Z. Hu, and T. Hui, "Low-Complexity Beamformer Design for Joint Radar and Communications Systems," *IEEE Communications Letters*, vol. 25, no. 1, pp. 259–263, 2021.
- [8] C. B. Barneto, T. Riihonen, M. Turunen, M. Koivisto, J. Talvitie, and M. Valkama, "Radio-based Sensing and Indoor Mapping with Millimeter-Wave 5G NR Signals," in *2020 International Conference on Localization and GNSS (ICL-GNSS)*, 2020, pp. 1–5.
- [9] 3GPP, "Physical channels and modulation," 3rd Generation Partnership Project (3GPP), Technical Specification (TS) 38.211, 1 2022, version 17.5.0. [Online]. Available: <https://portal.3gpp.org/desktopmodules/Specifications/SpecificationDetails.aspx?specificationId=3213>
- [10] J. Guan, A. Paidimarri, A. Valdes-Garcia, and B. Sadhu, "3-D Imaging Using Millimeter-Wave 5G Signal Reflections," *IEEE Transactions on Microwave Theory and Techniques*, vol. 69, no. 6, pp. 2936–2948, 2021.
- [11] 3GPP, "Study on New Radio (NR) access technology," 3rd Generation Partnership Project (3GPP), Technical Specification (TS) 38.912, 1 2022, version 17.5.0. [Online]. Available: <https://portal.3gpp.org/desktopmodules/Specifications/SpecificationDetails.aspx?specificationId=3059>
- [12] L. Bluestein, "A linear filtering approach to the computation of discrete Fourier transform," *IEEE Transactions on Audio and Electroacoustics*, vol. 18, no. 4, pp. 451–455, 1970.
- [13] M. Kottkamp, A. Pandey, D. Raddino, A. Roessler, and R. Stuhlfauth, "5G New Radio," *Fundamental Procedures and Technical Aspects*, 2019.
- [14] *MATLAB® 5G Toolbox™*. [Online]. Available: <https://www.mathworks.com/products/5g.html>